A Light Measurement Method for 9–150 kHz Disturbances in Power Grids Comparable to CISPR Quasi-Peak

Alexander Gallarreta, *Graduate Student Member, IEEE*, Igor Fernández, *Member, IEEE*, Deborah Ritzmann, Stefano Lodetti, Victor Khokhlov, *Member, IEEE*, Paul Wright, Jan Meyer, *Senior Member, IEEE*, and David de la Vega, *Senior Member, IEEE*

***Abstract*— This study proposes a novel measurement method to assess the disturbances in the electrical grid for the CISPR Band A (9–150 kHz), as no normative grid measurement method for these frequencies exists yet. Compatibility levels (CL) in IEC 61000-2-2 in this frequency range are defined based on the CISPR 16-1-1 method using the quasi-peak (QP) detector. However, this method is not directly applicable for grid measurements as it was originally designed for laboratory conditions and for measuring radio disturbances and immunity. The method proposed in this article (Light-QP method) overcomes these limitations, along with lower complexity, computational burden, and memory requirements than CISPR 16-1-1. The Light-QP method uses a digital QP detector that processes root mean square (rms) values of spectral components, calculated by adapting the IEC 61000-4-7 standard to the CISPR Band A. The proposed Light-QP method is applied to real measurements from a low-voltage (LV) distribution grid and compared to the QP outputs from a digital implementation of the CISPR 16-1-1 method. The results are comparable and can be used for assessment against CL. The Light-QP method has been presented to IEC SC77A/WG9 for its potential inclusion as a normative measurement method in a new version of the IEC 61000-4-30 standard.**

***Index Terms*— Electromagnetic interference, measurement techniques, power grids, power quality (PQ), smart grids, voltage measurement.**

I. Introduction

THE increasing penetration of renewable energy sources and modern energy-efficient technologies affects power quality (PQ) in the electrical grid and the performance of power line communications (PLC) used for smart grids [1]–[5]. In addition to classical harmonic distortion, a higher level of disturbances is observed in the frequency range from 9 to 150 kHz. These disturbances are mainly emissions caused by electronic devices based on inverters, such as electric vehicle (EV) chargers, photovoltaic (PV) inverters, modern power supplies, or battery chargers. These devices generate a set of high-level narrowband emissions at the switching frequencies and their harmonics in the range from 9 to 150 kHz [2]–[5]. Engines or lighting devices also generate high-level noise in frequencies up to 150 kHz [5], [6]. The increasing number of such devices leads to more frequent and higher (non-intentional) disturbances in the grid in frequencies currently used for data transmission by PLC (intentional emissions). As many of these electronic devices are close to smart meters for measuring consumption/generation (e.g., EV chargers and PV panel inverters), the emissions may affect the performance of the communications, impeding remote monitoring [2], [7].

Due to the historically limited presence of non-intentional distortion, the 9 to 150 kHz range has been lacking a comprehensive regulatory framework. However, with the increasing penetration of converter-based technologies in the grid, the need for regulation has led to new standardization. Immunity levels of equipment have been published in IEC 61000-4-19 [9], while compatibility levels (CL) that provide an upper bound for non-intentional and intentional grid disturbance levels are defined in IEC 61000-2-2 [10]. However, emission limits are still determined only for specific equipment [4], [5] and general limits for other appliances are under discussion within IEC CIS-H/JWG6.

A main limitation for proper EMC coordination, however, is the lack of a normative measurement method for disturbance levels in low-voltage (LV) power grids. Currently, only informative measurement methods for PQ measurements are suggested in the IEC 61000-4-30 standard [11], which are not mandatory for manufacturers and, consequently, measurements from different manufacturers are not directly comparable. The IEC SC77A/WG9 is currently working toward the definition of a normative method for measuring disturbances from 9 to 150 kHz in power grids. One of the candidates for becoming normative is the method specified in CISPR 16-1-1 [12], described in the form of a measuring receiver that is based on

Manuscript received 30 May 2022; revised 15 July 2022; accepted 20 July 2022. Date of publication 10 August 2022; date of current version 15 August 2022. This work was supported in part by the European Metrology Programme for Innovation and Research (EMPIR) Program under Project 18NRM05, in part by the Participating States and from the European Union's Horizon 2020 Research and Innovation Program, in part by the Spanish Government under Grant PID2021-124706OB-I00 (MCIU/AEI/FEDER-UE), in part by the Basque Government under Grant IT1436-22, and in part by the Pre-Doctoral (PREDOC) under Program PRE_2021_1_0006. The Associate Editor coordinating the review process was Dr. Grazia Barchi. *(Corresponding author: Alexander Gallarreta.)*

Alexander Gallarreta, Igor Fernández, and David de la Vega are with the Department of Communications Engineering, University of the Basque Country (UPV/EHU), 48013 Bilbao, Spain (e-mail: alexander.gallarreta@ehu.eus).

Deborah Ritzmann, Stefano Lodetti, and Paul Wright are with the National Physical Laboratory, Teddington TW11 0LW, U.K.

Victor Khokhlov and Jan Meyer are with the Institute of Electrical Power Systems and High Voltage Engineering, Technische Universität Dresden, 01062 Dresden, Germany.

Digital Object Identifier 10.1109/TIM.2022.3195255

different detectors, one of them the quasi-peak (QP) detector. The strongest argument for this method is that the CL are defined in IEC 61000-2-2 in terms of QP values [10], although for this decision grid measurements were not considered.

However, the CISPR 16-1-1 method presents the following drawbacks. First, it was introduced with the objective of protecting radio transmission from interference, and its suitability for the assessment of conducted disturbances in power grids raises some concerns. Second, the standard defines a method to measure QP values, but this is intended for laboratory measurements of Equipment Under Test (EUT), with a specific process of compliance assessment in a controlled environment [15]. Also, the description of the measuring receiver is based on an analog super-heterodyne receiver, which requires long measurement times. Implementation using digital processing is possible but not straightforward, with some non-mandatory guidance in the CISPR technical report [17] and specific published proposals [18], [19], in some instances with contradictory specifications on the type of window function, the overlap, and the frequency step size. Moreover, the CISPR 16-1-1 standard allows significant implementation flexibility, with accuracy requirements in the range of ± 2 dB (about $\pm 25\%$), wider than the accuracy of established PQ methods [12]; as a reference, the method for calculating root mean square (rms) values of disturbances for frequencies from 2 to 9 kHz determines an uncertainty limit of 10% [20]. Furthermore, measuring QP values has the disadvantage of being computationally complex, as they require a near-continuous reconstruction of the signal amplitude envelope in each frequency band [18]. Lastly, the CISPR 16-1-1 method does not provide rms values, which are commonly used for harmonics and interharmonics because they reflect the important interference mechanism of additional thermal stress. A measurement method that could give both rms and QP outputs could therefore be of great value for stakeholders involved in the electrical grid monitoring.

The motivation for the method presented in this article is to overcome the drawbacks of the CISPR 16 method in the context of grid application. For this purpose, this article proposes a new method for obtaining QP values, not bounded to laboratory conditions, and avoiding reproducibility issues, for direct comparison with CL. The new method is of low complexity and computational burden, such that it can be implemented on existing commercial instrumentation platforms for PQ field measurements. Additionally, a digital implementation of the CISPR 16-1-1 is proposed, which can be used as a reference tool for validation.

II. Objectives

This study aims to define a novel measurement method to assess the QP values of the disturbances in the LV grid for the CISPR Band A (from 9 to 150 kHz). The new method will be suitable for field measurements in the electrical grid, with no constraints that limit its use to controlled laboratory conditions. The complexity, the computational burden, and the memory requirements of the proposed measurement method must be significantly lower with respect to CISPR 16-1-1, to facilitate its implementation in simple and non-expensive instruments for on-field measurements. Based on these aspects, the proposed method is labeled "Light-QP." It is important to mention that the article does not propose a new detector, but a whole method adapted to be used in the grid. The aim is not to mimic the CISPR 16 receiver response, but achieving a reasonable similarity of the results, while being exactly reproducible.

Moreover, as there is no reference digital implementation of the CISPR 16-1-1 method, a specific configuration is defined and proposed in Section IV, compliant with the requirements of the standard.

The Light-QP method is based on a two-stage process: the first stage is an adaptation of the IEC 61000-4-7 method to the 9 to 150 kHz CISPR Band A, to obtain rms values of disturbance levels per 200 Hz band, with a frequency resolution of 100 Hz. These rms values are the input to the second stage, which is based on a digital QP detector that follows CISPR 16 guidance [12], and allows direct comparison with CL [10].

The combination of both outputs of the proposed method (rms and QP values) allows a more detailed characterization of the disturbances and their link to effects on equipment and installations as well as PLC. The rms amplitude is linked to thermal impact or appliances malfunctioning and other disturbances on PQ; the QP values are compared to CL defined in IEC 61000-2-2 to avoid interference effects on PLC [1], [12].

III. Existing Measurement Methods

A. Methods for the Assessment of Rms Values in the LV Grid

There is no normative method defined for rms measurements in the electrical grid for frequencies above 2 kHz. The IEC 61000-4-30 Annex C [11] proposes an "informative" method with a frequency resolution of 2 kHz, which does not allow comparison with CL, defined for 200 Hz resolution bandwidth [10], [21].

The CISPR 16-1-1 standard defines an "rms-Average" weighting detector, applicable to the 9 to 150 kHz range, defined as a critically damped meter that averages the frequency components to achieve a specific pulse response curve.

The method proposed in Annex B of the standard IEC 61000-4-7 [20] provides rms outputs with proper frequency resolution (200 Hz); however, it is defined as "informative" and only for frequencies between 2 and 9 kHz. Although it is intended to measure electronic equipment emissions, it can also be widely applied to assess disturbance levels in the field [21], [22]. The method specifies measurement intervals of 200 ms, using a rectangular window and data processing by Discrete Fourier Transform (DFT). Results are in the form of a discrete spectrum of rms values with 5 Hz frequency resolution. The spectral components are then grouped into 200 Hz bands using the rms. This grouping is "asymmetric" in frequency, since the frequency components considered for the assessment are not equally divided into lower and upper sides: 40 frequency components, in 5 Hz intervals, to assess a rms value each 200 Hz, considering 19 frequency components

below, and 20 above the center frequency. Nevertheless, the lack of a simple mathematical procedure that allows direct conversion of rms to QP values makes this method unsuitable to verify the CL. This method is also defined as "informative" in the standard [20] and, therefore, its implementation is not mandatory for compliance.

B. Methods for the Assessment of QP Values

The CL for the frequency range 9–150 kHz are defined in terms of QP values [10], which can be measured using a CISPR receiver [10], [12]. Nevertheless, the characteristics of this receiver are historically based on an analog superheterodyne receiver, which sequentially scans the frequency range. The QP detector is specified as an analog filter in series with a diode (non-linear element) and a critically damped meter. The elements of the filter are not specified by the standard, although suggestions for the corresponding time constants are given. The black-box approach of this standard and the wide allowed tolerances lead to several drawbacks already outlined in the introduction.

The CISPR TR 16-3 [17] is a technical report (not mandatory) of the CISPR 16 series with technical suggestions about the implementation of the standards. Among other aspects, it contains guidance for the digital implementation of the CISPR 16-1-1 receiver. Nevertheless, this guidance is not completely defined, and some practical questions and configurations remain open or still to be specified. For example, a method for measurements in the grid is not addressed in the CISPR 16 technical report. Therefore, in Section IV of this article, a digital implementation with fixed parameters of the CISPR 16-1-1 method is proposed, which solves the reproducibility issues and complies with the requirements and suggestions of the standard.

A DFT-based implementation of CISPR 16-1-1 is described in [18], to introduce some novel techniques in the development of digital receivers. In this proposal, the Lanczos kernel window function is used and digital filters to emulate the behavior of the analog circuits of the QP detector are proposed [18]. Nonetheless, this work does not provide specific implementation parameters for these filters, neither the equations to obtain the corresponding coefficients.

C. Other Methods

Other measurement methods have been recently proposed to evaluate the amplitude of disturbances in the electrical grid in the 9–150 kHz range [23]–[28]. A subsampling approach in [23] uses lower sampling rates for high frequencies, with a filter bank that decomposes the input signal into ten bands, which are processed by DFT assessment. A different approach is addressed by compressive sensing, where only the highest amplitude disturbances from a set of frequency bins of 2 kHz bandwidth are estimated through two different algorithms: Orthogonal Matching Pursuit Compressive Sensing [24] or Bayesian Compressive Sensing [25]. The Wavelet Packet Decomposition was also proposed by applying filtering and down-sampling recursively, where the measurement interval is synchronized to mains frequency [26].

As none of these methods provide QP results, they are not applicable for directly evaluating the significance of the grid disturbance levels with respect to CL. Additionally, the comparison of these methods reveals significant differences in the results [20], [27].

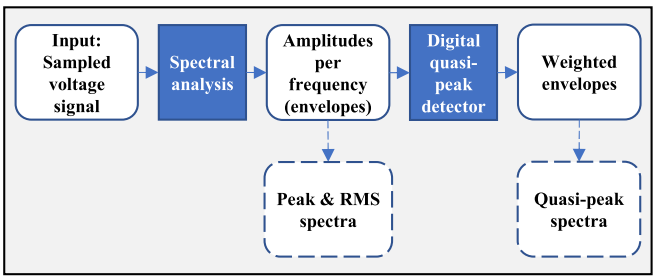

Fig. 1. Schematic of the digital implementation of CISPR 16-1-1 standard.

Recently, a method for emulating a CISPR 16 receiver has been published [28], based on a phase-locked loop. The method assumes that the emissions are sparse in the frequency domain and it is designed to identify only tonal or quasi-tonal high amplitude components [28]. Finally, some proposals for implementing a QP detector with the use of DFT and digital processing have been published [18], [19].

IV. Reference Digital Implementation of CISPR 16-1-1

Given the wide tolerances allowed by the standard [12], several compliant digital implementations of the CISPR 16-1-1 can be obtained, giving a wide range of results. To compare the performance of the newly proposed Light-QP method, a specific digital implementation of the CISPR 16-1-1 has been defined in this work and taken as reference.

In this section, the proposed implementation is detailed and the reasons behind the selection of the parameters are explained. This digital implementation has been defined following the CISPR 16-1-1 approach and the CISPR TR 16-3 guidelines. In particular, the informative annexes of CISPR 16-1-1 standard define the behavior of the analog circuitry, and the CISPR TR 16-3 provides some recommendations for the time windowing and the application of the Fourier analysis.

The proposed digital implementation of the CISPR 16-1-1 is based on a spectral analysis, including the overlapped windowing of the input data and a continuous STFT followed by a digital QP detector, as shown in Fig. 1.

The configuration selected to fulfill the specifications is the following:

1) A frequency step size of 50 Hz, equal to a quarter of the resolution bandwidth to avoid the "picket fence effect," in which the spectral shape of emissions can be lost when frequency components do not match the center frequencies of the frequency bands of the DFT, as proposed in CISPR TR 16-3 [17].
2) The frequency step size of 50 Hz implies the use of a window length of 20 ms.
3) A high degree of overlap between consecutive time windows is required to ensure the assessment of impulsive waveforms. In this implementation, an overlap of 90%

is applied, which corresponds to the minimum overlap proposed by CISPR TR 16-3 and it results in a time step of 2 ms between consecutive time windows.

4) The digital QP detector must follow the performance of a Resistor–Capacitor (*RC*) analog circuit and a critically damped meter, with charging, discharging and mechanical time constants defined in Annex H of CISPR 16-1-1 [12]. The digital QP detector has been implemented by means of Infinite Impulse Response (IIR) filters, as described analytically in Section V-B. A time step (T_e) of 2 ms is used to calculate the constants of the filters.
5) Lanczos kernel window with a –6 dB bandwidth (B_6) equal to 200 Hz is selected for the time windowing of the input data, as defined in DFT-based implementation of [18] (see Fig. 2), in line with CISPR 16-1-1 standard's frequency selectivity and the guidelines of CISPR TR 16-3.

Considering $w'[n]$ the Lanczos kernel window that fulfills the frequency response requirements in CISPR 16-1-1

$$w'[n] = \begin{cases} \text{sinc}(2(\frac{2n}{N-1}))\,\text{sinc}(\frac{2n}{N-1} - 1), & n \neq \frac{N-1}{2} \\ 1, & n = \frac{N-1}{2}. \end{cases} \quad (1)$$

Then, $w[n]$ can be defined as a discretized window function, defined as $w[n] = w'[n]/g$, for $n = 0, 1, \ldots, N-1, N$ being the number of samples per 20 ms window and $g = (1/N)\sum_{n=0}^{N-1} w'[n]$ being the coherent gain factor.

V. Definition of the Novel Light-QP Method

The Light-QP measurement method calculates QP values of the disturbances present in the grid for the 9–150 kHz frequency range, to allow the assessment against CL, as defined in IEC 61000-2-2.

The first stage is based on an rms measurement method adapted to the 9–150 kHz range, which provides the input values to a digital QP detector that follows the CISPR 16-1-1 guidance. The second stage of the method implements a digital QP detector based on the use of digital filters, which reproduce the analog behavior of both the *RC* circuit and the critically damped meter defined by the standard, as proposed in [19].

The method is based on a basic calculation interval of 3 s, which corresponds to the shortest aggregation interval as defined in IEC 61000-4-30. It also fulfills the 2 s minimum time required to obtain the initial QP output [11], [19]. The 3 s results provide the basis for aggregation over longer intervals (e.g., the most commonly used 10 min interval), as successive QP values can be obtained periodically from a sliding 3 s window. As the QP and rms values are obtained, the method provides a detailed spectral characterization of the grid disturbance.

A. Light-QP–Stage I: Computation of Rms Values in CISPR Band A

The first stage of the Light-QP method is based on IEC 61000-4-7–Annex B informative method (from 2 to 9 kHz), explained in Section III-A, with some adaptations to consider the particularities of CISPR 16-1-1 for Band A (from 9 to 150 kHz) and the characteristics of the emissions at these higher frequencies.

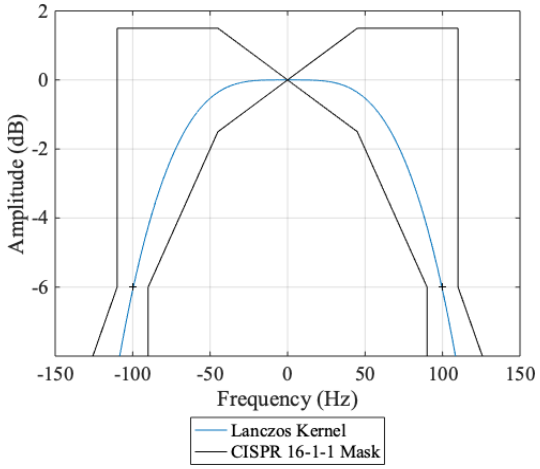

Fig. 2. Frequency response of the Lanczos kernel window function and CISPR 16-1-1 mask requirements.

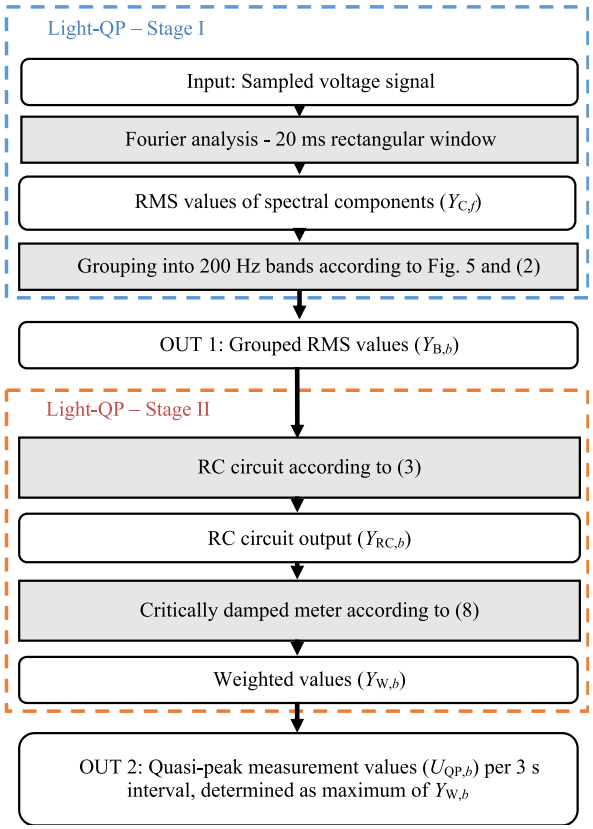

Fig. 3. Schematic overview of the Light-QP method.

The calculation procedure to apply the first stage of the Light-QP method is outlined in Fig. 3, which can be described with the following steps:

1) High-pass filter: the amplitudes of the fundamental and frequency components below 9 kHz must be attenuated to suppress spectral leakage, such that the dynamic range of the meter can be optimized to measure frequency

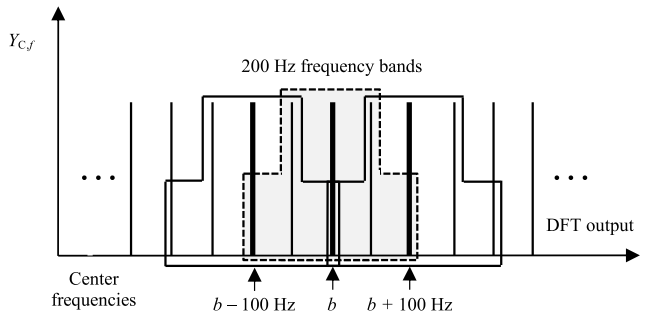

Fig. 4. Symmetrical grouping of 50 Hz frequency components into 200 Hz frequency bands.

components up to 150 kHz. A minimum attenuation of the fundamental component of 60 dB is recommended.

2) Fourier analysis: the STFT is applied to the sampled voltage signal to obtain the measured rms spectra. A shorter non-overlapped rectangular window of 20 ms length (instead of the 200 ms window defined in the IEC 61000-4-7 method) is used to compute the STFT. The shorter window allows the reduction of both the computational burden and the memory requirements for the DFT calculation. As a result, the output frequency components of DFTs have a frequency step size of 50 Hz.
3) Grouping of frequency components: the implemented technique overcomes the asymmetrical grouping of IEC 61000-4-7–Annex B method, described in Section III-A. A "symmetrical" grouping, in line with the harmonic grouping method defined for frequencies below 2 kHz in IEC 61000-4-7, is proposed for the frequency components generated by the DFT (see Fig. 4), which results in a resolution bandwidth of 200 Hz, in accordance with CISPR 16-1-1 and IEC 61000-2-2. Additionally, the assessment of frequency bands in multiples of 100 Hz is carried out in this step, which reduces the picket fence effect. As the resolution bandwidth is 200 Hz, it implies 50% overlap between adjacent frequency bands (see Fig. 4).

The detailed mathematical procedure of the first stage of the Light-QP involves, first, applying a DFT to the sampled input voltage, using a 20 ms rectangular window with no overlap. The output comprises rms values of spectral components $Y_{C,f}$, where f designates the frequency. As a result, the frequency step size between adjacent frequency components $Y_{C,f}$ is 50 Hz.

The rms values of spectral components $Y_{C,f}$ are then grouped in bands of 200 Hz (see Fig. 4). The output $Y_{B,b}$ (OUT 1 in Fig. 3) of each band is the rms value according to the following equation (2).

$$Y_{B,b} = \sqrt{\frac{1}{2}\cdot Y^2_{C,b-100\ \mathrm{Hz}} + \sum_{f=b-50\ \mathrm{Hz}}^{b+50\ \mathrm{Hz}} Y^2{}_{C,f} + \frac{1}{2}\cdot Y^2_{C,b+100\ \mathrm{Hz}}} \quad (2)$$

The center frequency b designates the band. The bands overlap by 100 Hz, with a separation between center frequencies of 100 Hz (b = 9.1, 9.2, …, 149.9 kHz).

TABLE I
IIR FILTER COEFFICIENT VALUES FOR THE *RC Circuit*

Coefficients	Charging process	Discharging process
b_0	1.8431×10^{-1}	0
b_1	1.8431×10^{-1}	1.9910×10^{-2}
a_1	-6.3138×10^{-1}	-9.6078×10^{-1}

The 200 Hz grouping has been chosen in accordance with the resolution bandwidth used in CISPR 16-1-1 Band A. The separation of 100 Hz results in overlapping 200 Hz bands, as shown in Fig. 4. Without this overlap, narrowband disturbances centered at the border between consecutive bands (e.g., 9.2, 9.4, and 9.6 kHz) would be split across two frequency bands, resulting in significantly lower measurement results than narrowband disturbances in the center of a band (e.g., 9.1, 9.3, and 9.5 kHz).

B. Light-QP Stage II: Digital Implementation of a QP Detector

The second stage of the Light-QP method consists of a digital QP detector, which reproduces the analog behavior of a *RC* circuit and a critically damped meter, as defined in CISPR 16-1-1 [12]. The implementation proposed in this article is performed through two IIR filters [19]. Hence, the analog *RC* circuit is modeled as a first-order linear system characterized by a charging and a discharging time constant, while the mechanical voltmeter is a critically damped second-order system characterized by the natural system frequency [19]. The charge and discharge time constants of the *RC* circuit are set to 45 and 500 ms, respectively, and the mechanical time constant for the critically damped meter is set to 160 ms, as recommended in the informative Annex H of CISPR 16-1-1 [12].

The output voltage $Y_{RC,b}[k]$ of the *RC* circuit is defined by the difference equation of a first-order IIR filter

$$Y_{RC,b}[k] = b_0 Y_{B,b}[k] + b_1 Y_{B,b}[k-1] - a_1 Y_{RC,b}[k-1] \quad (3)$$

where b_0, b_1, and a_1 are the filter coefficients.

The *RC* circuit may either be charging or discharging, depending on the relative magnitudes of input and output voltage

1) If $Y_{RC,b}[k\text{-}1] \leq Y_{C,b}[k]$, then coefficients b_0, b_1, and a_1 are set according to a time constant of 45 ms for charging.
2) If $Y_{RC,b}[k\text{-}1] > Y_{C,b}[k]$, then $b_0 = 0$, and b_1, a_1 are set according to a time constant of 500 ms for discharging.

The filter coefficient values are listed in Table I, determined from the analog time constants and the use of the bilinear approximation as described below.

The analog cut-off frequency is defined in terms of an analog time constant τ_{RC} of the *RC* circuit

$$\Omega_{\text{cut-off}} = 1/\tau_{RC}. \quad (4)$$

A pre-warped coefficient is defined for the bilinear approximation

$$s = \frac{1}{\tan(\Omega_{\text{cut-off}} \cdot T_e/2)} \quad (5)$$

TABLE II
IIR FILTER COEFFICIENT VALUES FOR THE RC CIRCUIT

Coefficients	Discharging process
$b_{0,\mathrm{m}}$	3.4687×10^{-3}
$b_{1,\mathrm{m}}$	6.9374×10^{-3}
$b_{2,\mathrm{m}}$	3.4687×10^{-3}
$a_{1,\mathrm{m}}$	-1.7644
$a_{2,\mathrm{m}}$	7.7829×10^{-1}

where $T_e = 20$ ms is the time step between consecutive rms values $Y_{\mathrm{B},b}[k]$ of the spectral components.

The filter coefficients b_0, b_1, and a_1 are then calculated as

$$b_0 = b_1 = \frac{1}{1+s} \tag{6}$$

$$a_1 = \frac{1-s}{1+s}. \tag{7}$$

The *RC* circuit output $Y_{\mathrm{RC},b}[k]$ is further processed with a critically damped mechanical meter, modeled as a second-order IIR filter, to calculate weighted rms values $Y_{\mathrm{W},b}[k]$ of spectral components

$$\begin{aligned} Y_{\mathrm{W},b}[k] = {} & b_{0,\,\mathrm{m}} Y_{\mathrm{RC},b}[k] + b_{1,\,\mathrm{m}} Y_{\mathrm{RC},b}[k-1] \\ & + b_{2,\,\mathrm{m}} Y_{\mathrm{RC},b}[k-2] \\ & - a_{1,\,\mathrm{m}} Y_{\mathrm{W},b}[k-1] - a_{2,\,\mathrm{m}} Y_{\mathrm{W},b}[k-2]. \end{aligned} \tag{8}$$

Filter coefficients $b_{0,\mathrm{m}}$, $b_{1,\mathrm{m}}$, $b_{2,\mathrm{m}}$, $a_{1,\mathrm{m}}$, and $a_{2,\mathrm{m}}$ are set according to an analog angular time constant of 160 ms. Table II lists the coefficients of the digital IIR filters related to this constant, which are determined by bilinear approximation.

The analog angular cut-off frequency $\Omega_n = 1/\tau_{\mathrm{W}}$ is defined in terms of the time constant τ of the critically damped meter to apply the bilinear approximation. The corrected analog cut-off frequency for the critically damped meter is

$$f_n = \Omega_n / 2\pi. \tag{9}$$

The digital angular cut-off frequency s_0 is defined as

$$s_0 = \tan(\pi \cdot f_n \cdot T_e). \tag{10}$$

As a result, the second-order IIR digital filter coefficients are defined as

$$b_{0,\,\mathrm{m}} = b_{2,\,\mathrm{m}} = \frac{s_0^2}{s_0^2 + 2 \cdot s_0 + 1} \tag{11}$$

$$b_{1,\,\mathrm{m}} = 2 \cdot b_{0,\,\mathrm{m}} \tag{12}$$

$$a_{1,\,\mathrm{m}} = -2 \cdot b_{0,\,\mathrm{m}} \cdot (1/s_0^2 - 1) \tag{13}$$

$$a_{2,\,\mathrm{m}} = -\big(1 - \big(b_{0,\,\mathrm{m}} + b_{1,\,\mathrm{m}} + b_{2,\,\mathrm{m}} - a_{1,\,\mathrm{m}}\big)\big). \tag{14}$$

Lastly, the QP outputs $U_{\mathrm{QP,b}}$ (OUT 2 in Fig. 3) are determined by the maximum of the weighted values $Y_{\mathrm{W},b}[k]$ of the spectral components with center frequency b. The first output requires an initial assessment interval of 3 s, which fulfills the 2 s required to obtain the initial QP output [19]. Subsequent QP values could be determined periodically every 20 ms from a sliding 3 s window; another option is to apply the method per 3 s aggregation intervals, provided that the variables of the QP detector ($Y_{\mathrm{B},b}$, $Y_{\mathrm{RC},b}$, and $Y_{\mathrm{W},b}$) obtained at the end of each 3 s interval are applied to the next interval.

VI. EVALUATION OF THE LIGHT-QP METHOD

In this section, the proposed method is evaluated according to the following aspects: computational burden, memory requirements and accuracy. For this evaluation, the proposed method is compared to the digital implementation of the CISPR 16-1-1 method described in Section IV.

A. Computational Burden and Memory Requirements

The computational burden and the memory requirements needed to assess the QP values up to 150 kHz for a basic time interval of 3 s have been quantified, and results are summarized in Table III. Moreover, both methods have been applied in the same computer under the same conditions to provide an estimation of the processing time (MacBook Pro, CPU 2.6 GHz Intel Core i5 dual core, RAM 8 GB 1600 MHz DDR3, and MATLAB R2019b). Although the calculation times for CISPR 16 can be reduced through software and hardware optimization (e.g., with the use of field-programmable gate arrays), the table provides an indication of the difference in computational complexity.

Results show that the computational burden, in terms of the number of FFTs, is $10\times$ lower for Light-QP. Moreover, the memory requirements are more than $100\times$ lower for calculating the spectrogram (matrix of intermediate results in time and frequency domains) and more than $10\times$ lower for obtaining QP outputs. Although the processing times depend significantly on the hardware platform, the figures in the table about processing times demonstrate the reduced complexity of the Light-QP method with respect to the resources required by the digital implementation in accordance with the requirements of the CISPR 16-1-1 standard. The digital implementation according to CISPR 16-1-1 (Section IV) entails a high-computational cost because it emulates the continuous time response of the analog equipment. This requires highly overlapped FFTs (see Table III), which imply very resource-intensive effort to provide quasi-continuous output.

The significantly lower demand of resources, together with the lower complexity, are a clear demonstration of the lower hardware requirements to implement the Light-QP method in PQ devices and commercial instruments for field measurements in the grid.

B. Comparison of Methods

The outputs of the Light-QP method have been compared to the results of the digital CISPR 16-1-1 implementation defined in Section IV. For the evaluation, a comprehensive set of 29 recordings of disturbances in the LV grid representing different types of noise and disturbances, together with PLC transmission bursts, have been used. Most of them (20) are field measurements in different rural and urban scenarios in Spain, selected by the distribution system operator (DSO) as representative examples of rural and urban distribution grid topologies in Spain [3]. Nine recordings are measured at the point of connection (POC) of PV inverters and EV chargers to the grid, measured in Spain and Germany [22]. These recordings are considered as the most relevant cases where CL may be exceeded.

TABLE III
COMPUTATIONAL REQUIREMENTS OF LIGHT-QP METHOD

Method	Time step	Number of FFT	Memory (QP output)	Memory (spectrogram)	Elapsed real time	CPU processing time
Digital CISPR 16	2 ms	1491	0.68 MB	203.23 MB	6.60 s	9.83 s
Light-QP	20 ms	150	0.06 MB	1.77 MB	0.31 s	0.57 s

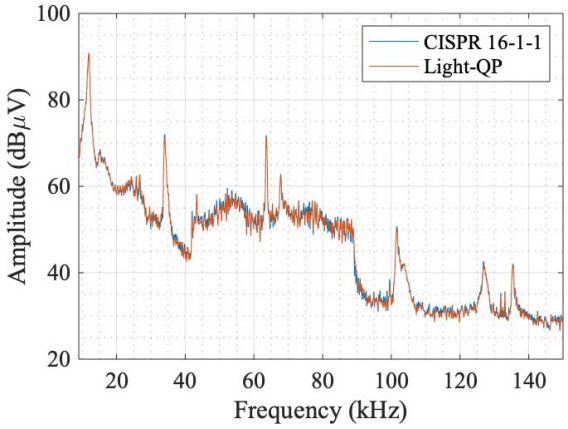

Fig. 5. Outputs of Light-QP and digital CISPR 16-1-1 measurement methods for a LV grid measurement.

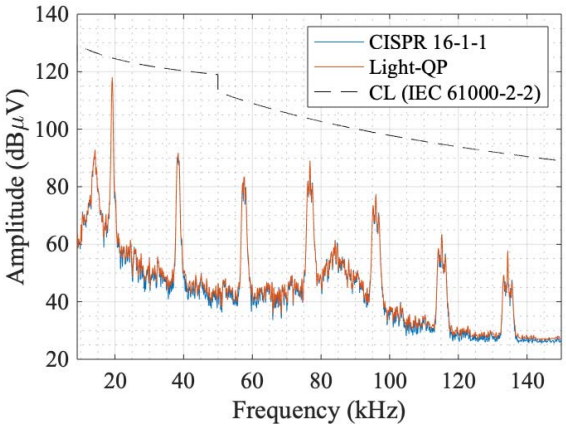

Fig. 6. Outputs of Light-QP and digital CISPR 16-1-1 measurement methods for a PV inverter measurement with compatibility levels (CL) of IEC 61000-2-2.

For the signals recorded in Spain, the acquisition system was composed of a voltage probe, a high-resolution oscilloscope and a laptop to automatize the measurement [3]. The voltage probe implements a 10–500 kHz bandpass filter to avoid the mains and to protect the equipment, with a flat response for the whole frequency band of interest and for the whole range of expected LV access impedance values [30]. The oscilloscope is configured with an 8.92 MHz sampling rate and an amplitude resolution of 16 bit/Sample. The filtering of the mains allows to focus the amplitude resolution of the acquisition system on the level of the disturbances.

In the measurements performed in Germany, the raw data were recorded continuously using a transient recorder, composed of a 16-bit resolution analog-to-digital converter, with 1 MHz of sampling rate. Before sampling the voltage signal, an analog Butterworth low-pass filter with the cut-off frequency of 300 kHz was used to prevent the aliasing effect. Finally, a digital high-pass filter was applied to the raw data to reduce spectral leakage by damping the fundamental component and low-order harmonics from the input signal [31].

Fig. 5 shows an example of the outputs of Light-QP and digital CISPR 16-1-1 methods for a measurement in the LV distribution grid. The emissions in the figure are generated by PLC transmissions (in the range from 40 to 90 kHz) and by electronic devices that inject high-level narrowband disturbances at different frequencies within this range.

The comparison of the disturbance levels at connection points of PV inverters and EV chargers against CL is an important use case, especially for utilities. The waveforms generated by these devices usually show high amplitude, which are close to the limits of CL. Fig. 6 shows the spectrum of a measurement taken at the POC of a PV inverter, computed with CISPR 16-1-1 and Light-QP methods, with respect to the CL defined in IEC 61000-2-2. Table IV summarizes the relative differences between CISPR 16-1-1 and Light-QP for the six highest peaks of the disturbances in this use case. Results show that Light-QP is a suitable measurement method to evaluate the emissions from inverters, since differences in the peaks with respect to the digital CISPR 16-1-1 are between 0.1% and 2.3%. To put this difference into context, different implementations of CISPR 16 can give a spread in results of ±25% from each other. The target accuracy for these PQ measurements is ±10%.

TABLE IV
RELATIVE DIFFERENCES OF WAVEFORMS WITH HIGHER AMPLITUDE

Frequency band	Relative diff.	Frequency band	Relative diff.
14.2 kHz	0.57 %	57.6 kHz	0.46 %
19.2 kHz	2.27 %	76.8 kHz	1.37 %
38.4 kHz	0.12 %	96.0 kHz	2.27 %

The outputs of both methods for the same input signals are compared every 100 Hz, and quantified by the median value of the differences ($U_{\mathrm{QP}-C16,b}U_{\mathrm{QP},b}$), in absolute value and in percentage, with respect to the CISPR 16-1-1 output. The standard deviation of the modulus is also calculated, according to the following equation:

$$\sigma = \sqrt{\frac{1}{N}\left(\sum_{b=1}^{N}(U_{\mathrm{QP-C16},b} - U_{\mathrm{QP},b} - \bar{X})^2\right)} \qquad (15)$$

where N is the number of frequency bands, $U_{\mathrm{QP}-C16,b}$ is the QP result of the digital implementation CISPR 16-1-1, while $U_{\mathrm{QP},b}$ are the QP values obtained with the Light-QP method and $\overline{X}$ is the mean value of differences ($U_{\mathrm{QP}-C16,b}U_{\mathrm{QP},b}$).

TABLE V
COMPARISON OF LIGHT-QP AND CISPR 16-1-1 OUTPUTS

	Absol. value of diff.		Relative diff.	Relative diff. w.r.t. compatib. levels	
	Median	St. Dev.	Median	Freq. bands with diff. < 2% of CL	Freq. bands with diff. < 10% of CL
All the frequency bands in all the signals	$-3.1\text{x}10^{-4}$ mV	1.16 mV	7.16 %	99.68 %	99.98 %
Frequency bands of the 50 highest values of each signal	0.26 mV	5.83 mV	5.56 %	96.07 %	99.52 %

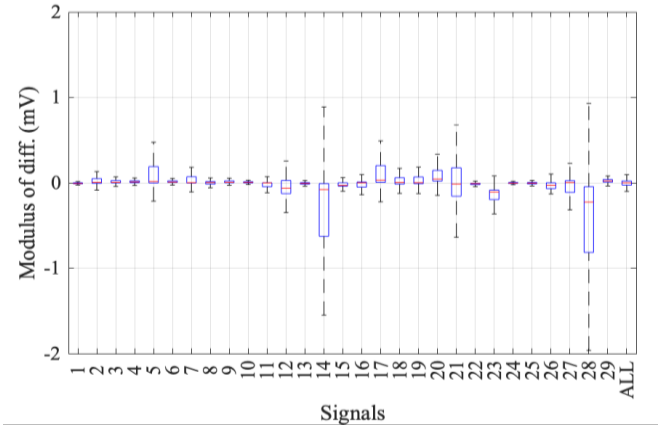

Fig. 7. Differences, in absolute values, between Light-QP and CISPR 16 1 1 outputs for each of the 29 test recordings and for the total of the recordings.

Results of this statistical analysis for the same input data are depicted in Table V. The frequency bands of the 50 highest values of each signal have been considered separately, as one of the main interests of the method is the measurement of the highest disturbances for comparison with CL. For all the frequency bands, the results show that the median of the differences is below 1 μV, a small quantity relative to CL, which range from 2.98 V at 9 kHz to 28 mV at 150 kHz [10]. In percentage, the median value of the differences is within the accuracy requirements for rms assessment (10%) [11], and considerably lower than the ± 2 dB tolerances (about $\pm 25\%$) defined for the CISPR 16-1-1 receiver [12]. The absolute values of the differences between both measurement methods for the grid recordings used for the accuracy assessment of the proposed method are plotted in the boxplot of Fig. 7. As it can be observed in the figure illustrates, the differences for most of recordings are within ± 0.5 mV, and the highest differences are between -2 and $+1$ mV. The results for the frequency bands containing the highest values of emissions are also below 1 mV in absolute value and below 10% of relative difference.

Considering that the final aim of the proposed method is to assess the grid disturbance levels with respect to the CL, the differences of the outputs of both methods are also evaluated considering the CL as a reference. As the CL are defined as a function of the frequency, from 2.98 V at 9 kHz to 28 mV at 150 kHz [10], this comparison is performed for each frequency band. Hence, the difference between both methods is compared to the CL value of the corresponding frequency band, in the form of percentage of the CL value. Finally, the percentage of the frequency bands where the difference is lower than a specific limit (2% and 10% of the corresponding CL) is quantified (see Table V, columns on the right). The comparison shows that outputs of both methods differ less than 2%, with respect to the corresponding CL for 99.68% of the frequency bands, and less than 10% for 99.98% of the frequency bands. For the highest disturbances, the 96.07% and 99.52% of the frequency bands differ less than 2% and 10% with respect to the corresponding CL, respectively. These outcomes demonstrate that the results of the Light-QP method allow for assessment of disturbance levels against CL with accuracy comparable to a digital CISPR 16-1-1 implementation.

VII. CONCLUSION

The assessment of LV grid disturbance levels in the frequency range from 9 to 150 kHz with respect to CL as defined in IEC 61000-2-2 requires QP measurement values. The only available method recommended by the IEC 61000-4-30 Ed. Three to measure QP values is the CISPR 16-1-1 standard. However, this standard was not designed for PQ grid measurements, but to evaluate interference with radio transmission. The normative implementation allows high tolerances (± 2 dB, which corresponds to about $\pm 25\%$) and requires high-computational performance and memory requirements.

In this article, a novel measurement method for the assessment of disturbances in the electrical grid for the frequency range from 9 to 150 kHz is proposed. The new method (Light-QP) addresses the lack of a normative method for grid measurements in this frequency range, with the purpose of providing QP values that can be directly compared to CL. The Light-QP method includes a compliant implementation of a QP detector; the main differences with respect to the standard are in the pre-detector stages, which determine the computational complexity. Hence, the Light-QP significantly reduces the computational burden and memory requirements with respect to CISPR 16-1-1, which is a key aspect for PQ surveys that require continuous measurements over at least one week. This aspect allows the implementation of the new method in non-expensive PQ instruments for field measurements in the distribution grid, with respect to the present generation of measurement instruments. The lower resources requirements are mainly achieved with a new method for calculating the rms values (which are the input data for the QP calculation), based on a non-overlapping rectangular DFT window and symmetrical grouping of the frequency components. Moreover, a digital

QP detector is implemented by means of two IIR filters, which follow CISPR 16-1-1 recommendations. The new method is not equivalent nor calibrated according to CISPR 16 test procedures, but it gives results comparable to the CISPR 16-1-1 receiver for commonly observed characteristics in grid measurements. The specific configuration of the method avoids ambiguity in the method implementation, wide tolerances, and ensures high reproducibility. Moreover, it avoids the pre-scan measurement techniques to give a fast and approximated view of the disturbance levels. In this line, the method allows the implementation of a procedure similar to pre-scan, but looking at maximum values, which can be recorded together with QP outputs.

The results in the form of rms, maximum and QP values allow more holistic evaluation of the most common interference mechanisms in these frequencies, since the rms values are related to the power of the emission in PQ (thermal impact and malfunctions), and the QP values with a 200 Hz resolution bandwidth can be used for comparison with CL and evaluation of the impact on PLC.

The Light-QP method has been presented to IEC SC77A/WG9 and discussed for its potential inclusion as a normative measurement method in a new edition of the IEC 61000-4-30 standard.

REFERENCES

[1] S. K. Rönnberg *et al.*, "On waveform distortion in the frequency range of 2 kHz–150 kHz—Review and research challenges," *Electr. Power Syst. Res.*, vol. 150, pp. 1–10, Sep. 2017.

[2] N. Uribe-Pérez, I. Angulo, L. Hernández-Callejo, T. Arzuaga, D. de la Vega, and A. Arrinda, "Study of unwanted emissions in the CENELEC—A band generated by distributed energy resources and their influence over narrow band power line communications," *Energies*, vol. 9, no. 12, p. 1007, Nov. 2016.

[3] I. Fernández, D. de la Vega, A. Arrinda, I. Angulo, N. Uribe-Pérez, and A. Llano, "Field trials for the characterization of non-intentional emissions at low-voltage grid in the frequency range assigned to NB-PLC technologies," *Electronics*, vol. 8, no. 9, p. 1044, Sep. 2019.

[4] G. F. Bartak and A. Abart, "EMI of emissions in the frequency range 2 kHz–150 kHz," in *Proc. 22nd Int. Conf. Exhib. Electr. Distrib. (CIRED)*, Jun. 2013, pp. 10–13.

[5] I. Fernandez *et al.*, "Characterization of non-intentional emissions from distributed energy resources up to 500 kHz: A case study in Spain," *Int. J. Electr. Power Energy Syst.*, vol. 105, pp. 549–563, Feb. 2019.

[6] L. C. Long, W. E. Sayed, V. Munesswaran, N. Moonen, R. Smolenski, and P. Lezynski, "Assessment of conducted emission for multiple compact fluorescent lamps in various grid topology," *Electronics*, vol. 10, no. 18, p. 2258, Sep. 2021.

[7] S. Galli, A. Scaglione, and Z. Wang, "For the grid and through the grid: The role of power line communications in the smart grid," *Proc. IEEE*, vol. 99, no. 6, pp. 998–1027, Jun. 2011, doi: 10.1109/JPROC.2011.2109670.

[8] *Investigation Results on Electromagnetic Interference in the Frequency Range Below 150 kHz*, document CLC/TR 50669, CENELEC SC 205A, 2017.

[9] *Electromagnetic Compatibility (EMC)—Part 4-19: Testing and Measurement Techniques Test for Immunity to Conducted, Differential Mode Disturbances and Signalling in the Frequency Range 2 kHz to 150 kHz at A.C. Power Ports*, document IEC 61000-4-19, International Electrotechnical Commission, 2014.

[10] *Electromagnetic Compatibility (EMC)—Part 2–2: Environment Compatibility Levels for Low-Frequency Conducted Disturbances and Signalling in Public Low-Voltage Power Supply Systems*, document IEC 61000-2-2:2002+AMD1:2017+AMD2, International Electrotechnical Commission, 2018.

[11] *Electromagnetic Compatibility (EMC)—Part 4–30: Testing and Measurement Techniques Power Quality Measurement Methods*, document IEC 61000-4-30 Ed.3, International Electrotechnical Commission, 2015.

[12] *Specification for Radio Disturbance and Immunity Measuring Apparatus and Methods—Part 1–1: Radio Disturbance and Immunity Measuring Apparatus Measuring Apparatus*, document CISPR 16-1-1, CISPR, 2019.

[13] M. A. Azpurua, M. Pous, and F. Silva, "Specifying the waveforms for the calibration of CISPR 16-1-1 measuring receivers," *IEEE Trans. Electromagn. Compat.*, vol. 62, no. 3, pp. 654–662, Jun. 2020, doi: 10.1109/TEMC.2019.2923813.

[14] M. A. Azpurua, M. Pous, J. A. Oliva, B. Pinter, M. Hudlicka, and F. Silva, "Waveform approach for assessing conformity of CISPR 16–1–1 measuring receivers," *IEEE Trans. Instrum. Meas.*, vol. 67, no. 5, pp. 1187–1198, May 2018, doi: 10.1109/TIM.2018.2794941.

[15] *Specification for Radio Disturbance and Immunity Measuring Apparatus and Methods—Part 2-1: Methods of Measurement of Disturbances and Immunity Conducted Disturbance Measurements*, document CISPR 16-2-1, CISPR, 2014.

[16] M. Monti, E. Puri, and M. Monti, "Hidden aspects in CISPR 16–1–1 full compliant fast Fourier transform EMI receivers," in *Proc. Int. Symp. Electromagn. Compat. EMC Eur.*, Sep. 2016, pp. 34–39, doi: 10.1109/EMCEurope.2016.7739159.

[17] *Specification for Radio Disturbance and Immunity Measuring Apparatus and Methods—Part 3: CISPR Technical Reports*, document CISPR/TR 16-3:2010+A2, CISPR, 2015.

[18] M. Schwenke and D. Klingbeil, "Application aspects and measurement methods in the frequency range from 9 kHz to 150 kHz," in *Proc. 25th Int. Conf. Electr. Distrib. (CIRED)*, Jun. 2019, pp. 3–6.

[19] F. Krug and P. Russer, "Quasi-peak detector model for a time-domain measurement system," *IEEE Trans. Electromagn. Compat.*, vol. 47, no. 2, pp. 320–326, May 2005, doi: 10.1109/TEMC.2005.847410.

[20] *Electromagnetic Compatibility (EMC)—Part 4–7: Testing and Measurement Techniques General Guide on Harmonics and Interharmonics Measurements and Instrumentation, for Power Supply Systems and Equipment Connected Thereto*, document IEC 61000-4-7:2002+AMD1, International Electrotechnical Commission, 2008.

[21] V. Khokhlov, J. Meyer, A. Grevener, T. Busatto, and S. Ronnberg, "Comparison of measurement methods for the frequency range 2–150 kHz (Supraharmonics) based on the present standards framework," *IEEE Access*, vol. 8, pp. 77618–77630, 2020.

[22] V. Khokhlov, J. Meyer, D. Ritzmann, S. Lodetti, P. S. Wright, and D. de la Vega, "Application of measurement methods for the frequency range 2-150 kHz to long-term measurements in public low voltage networks," in *Proc. Int. Conf. (CIRED)*. Geneva, Switzerland, Sep. 2021, pp. 1–5.

[23] T. M. Mendes, C. A. Duque, L. R. M. Silva, D. D. Ferreira, and J. Meyer, "Supraharmonic analysis by filter bank and compressive sensing," *Electric Power Syst. Res.*, vol. 169, pp. 105–114, Apr. 2019.

[24] S. Zhuang, W. Zhao, R. Wang, Q. Wang, and S. Huang, "New measurement algorithm for supraharmonics based on multiple measurement vectors model and orthogonal matching pursuit," *IEEE Trans. Instrum. Meas.*, vol. 68, no. 6, pp. 1671–1679, Jun. 2019.

[25] S. Zhuang, W. Zhao, Q. Wang, Z. Wang, L. Chen, and S. Huang, "A high-resolution algorithm for supraharmonic analysis based on multiple measurement vectors and Bayesian compressive sensing," *Energies*, vol. 12, no. 13, p. 2559, Jul. 2019.

[26] S. Lodetti, J. Bruna, J. J. Melero, V. Khokhlov, and J. Meyer, "A robust wavelet-based hybrid method for the simultaneous measurement of harmonic and supraharmonic distortion," *IEEE Trans. Instrum. Meas.*, vol. 69, no. 9, pp. 6704–6712, Sep. 2020.

[27] D. Ritzmann *et al.*, "Comparison of measurement methods for 2–150-kHz conducted emissions in power networks," *IEEE Trans. Instrum. Meas.*, vol. 70, pp. 1–10, 2021, doi: 10.1109/TIM.2020.3039302.

[28] T. M. Mendes, D. D. Ferreira, L. R. M. Silva, P. F. Ribeiro, J. Meyer, and C. A. Duque, "PLL based method for supraharmonics emission assessment," *IEEE Trans. Power Del.*, vol. 37, no. 4, pp. 2610–2620, Aug. 2022, doi: 10.1109/TPWRD.2021.3112404.

[29] A. J. Collin, S. Z. Djokic, J. Drapela, R. Langella, and A. Testa, "Proposal of a desynchronized processing technique for assessing high-frequency distortion in power systems," *IEEE Trans. Instrum. Meas.*, vol. 68, no. 10, pp. 3883–3891, Oct. 2019.

[30] I. Fernández, M. Alberro, J. Montalbán, A. Arrinda, I. Angulo, and D. de la Vega, "A new voltage probe with improved performance at the 10 kHz–500 kHz frequency range for field measurements in LV networks," *Measurement*, vol. 145, pp. 519–524, Oct. 2019, doi: 10.1016/j.measurement.2019.05.106.

[31] M. Klatt, J. Meyer, P. Schegner, R. Wolf, and B. Wittenberg, "Filter for the measurement of supraharmonics in public low voltage networks," in *Proc. IEEE Int. Symp. Electromagn. Compat. (EMC)*, Aug. 2015, pp. 108–113, doi: 10.1109/ISEMC.2015.7256141.

Alexander Gallarreta (Graduate Student Member, IEEE) received the B.Sc. and M.Sc. degrees in telecommunications engineering from the University of the Basque Country (UPV/EHU), Bilbao, Spain, in 2019 and 2021, respectively, where he is currently pursuing the Ph.D. degree in mobile network information and communication technologies.

His current research is focused on signal processing for the analysis of low-voltage grid emissions measurement methods.

Igor Fernández (Member, IEEE) received the M.Sc. and Ph.D. degrees in telecommunication engineering from the University of the Basque Country (UPV/EHU), Bilbao, Spain, in 2001 and 2011, respectively.

He is currently an Assistant Professor with the Department of Communications Engineering, UPV/EHU. His current research interests focus on new digital broadcasting technologies and power line communications (PLC).

Deborah Ritzmann received the B.Sc. degree in mathematics and physics from the University College London, London, U.K., in 2012, and the Ph.D. degree in electronic engineering from the University of Reading, Reading, U.K., in 2017.

She subsequently worked with National Grid ESO, Warwick, U.K., and a Renewable Generation Developer with Anesco, Reading. She joined the National Physical Laboratory, Teddington, U.K., in 2019, where she is currently a Senior Research Scientist specializing in power networks metrology.

Stefano Lodetti received the B.Sc. and M.Sc. degrees in physics from the University of Milan, Milan, Italy, in 2012 and 2015, respectively, and the Ph.D. degree in renewable energies and energy efficiency from the University of Zaragoza, Zaragoza, Spain, in 2020.

From 2016 to 2019 he was a Researcher with Fundación CIRCE, Zaragoza, Spain. Since 2020, he has been as a Higher Research Scientist with the National Physical Laboratory, Teddington, U.K. His research interests are power systems measurements and power quality.

Victor Khokhlov (Member, IEEE) received the B.Sc. degree in electrical power engineering from the Moscow Power Engineering Institute, Moscow, Russia, in 2014, and the M.Sc. degree in electrical power engineering from the Ilmenau University of Technology, Ilmenau, Germany, in 2017. He is currently pursuing the Ph.D. degree in electrical power engineering with the Institute of Electrical Power Systems and High Voltage Engineering, Technische Universität Dresden, Dresden, Germany.

His research interest includes different aspects of network disturbances above 2 kHz, especially their impact on functionality and lifetime of modern electrical appliances.

Paul Wright received the B.Sc. and Ph.D. degrees in electrical and electronic engineering from the University of Surrey, Surrey, U.K., in 1987 and 2002, respectively.

He spent three years as a Research Fellow with the University of Surrey, Guildford, U.K., where he was involved in the field of spacecraft sensors and attitude control. This was followed by three years with the Central Electricity Research Laboratory, Leatherhead, Surrey, where he was involved in advanced control systems. In 1992, he joined the National Physical Laboratory, Teddington, U.K., where he is currently a Principal Research Scientist specializing in ac measurements and waveform analysis. He has coordinated five EU Collaborative Research and Development Projects and he is currently a Coordinator of the EU project on 2–150 kHz grid measurement SupraEMI of which this work is part.

Jan Meyer (Senior Member, IEEE) received the Dipl.-Ing. and Ph.D. degrees in electrical power engineering and the Ph.D. degree in power quality from Technische Universität Dresden, Dresden, Germany, in 1994, 2004, and 2018, respectively.

He is currently with Technische Universität Dresden as a Senior Lecturer and Team Leader of the Power Quality Research Group. His research interests include network disturbances and their assessment, especially for distortion below and above 2 kHz, methods and accuracy of Power Quality measurements, and analyzing big data amounts from Power Quality measurement campaigns.

Dr. Meyer is a member of several national and international working groups on electromagnetic compatibility (EMC) standardization and active in Conseil International des Grands Réseaux Électriques (CIGRE) and International Conference and Exhibition on Electricity Distribution (CIRED).

David de la Vega (Senior Member, IEEE) received the M.Sc. and Ph.D. degrees in telecommunication engineering from the University of the Basque Country (UPV/EHU), Bilbao, Spain, in 1996 and 2008, respectively.

He is currently an Associate Professor with the Department of Communications Engineering, UPV/EHU. His current research is focused on the analysis of signal propagation on smart grids.